IEEE Transactions on Power Electronics, Vol 8., No. 4, pp. 4235-4240, April 2023.

Core Energy Capacitance of NiZn Inductors

Zhan Shen, *Member, IEEE*, Wu Chen, *Senior Member, IEEE*, Hongbo Zhao, *Member, IEEE*, Long Jin, Alex J. Hanson, *Member, IEEE*, David J. Perreault, *Fellow, IEEE*, and Charles R. Sullivan, *Fellow, IEEE*, Frede Blaabjerg, *Fellow, IEEE*, and Huai Wang, *Senior Member, IEEE*

***Abstract*—In the high-frequency (HF, 3–30 MHz) range, NiZn cores are commonly used. They have much lower permeability and permittivity than materials typically used at lower frequencies, including MnZn ferrites. Previously-used capacitance models rely on the Perfect Electrical Conductor assumption. They are not applicable when NiZn cores are used. We propose a general core energy capacitance model found by solving the electric field boundary value problem. We also propose a simplified model by curve fitting to FEA data. Both are verified by simulation and experimental results in two case studies with rod and pot core structures.**

***Index Terms*—Stray capacitance, core energy capacitance, high-frequency inductor, NiZn ferrite, magentics.**

I. Introduction

The demands of small size and light weight push the design of power electronics to higher switching frequencies. More and more designs entering the HF (3–30 MHz) region [1]. As switching frequencies increase, the stray capacitance of magnetic components becomes more important. Stray capacitance limits the converter's operating frequency, leads to current ringing, and contributes to electromagnetic interference (EMI) [2]. Accurately modeling parasitic capacitance is therefore essential in order to reduce it by design.

Inductor capacitance C_{ind} is typically modeled as the sum of a winding-related capacitance C_{w} and a core-related capacitance C_{core}, which is illustrated in Fig. 1(a). C_{core} includes capacitances that account for energy stored in between the core and the winding C_{cw}, and energy stored in the core itself C_{ce}. When applying a certain voltage across the inductor, those stored energies and corresponding capacitors are added across the inductor terminals, as shown in the equivalent circuit in Fig. 1(c). There are extensive studies of C_{w} and C_{cw} [3–6]. C_{w} represents the electric energy storage capability of the winding, and relates to the wire diameter, insulation, and air

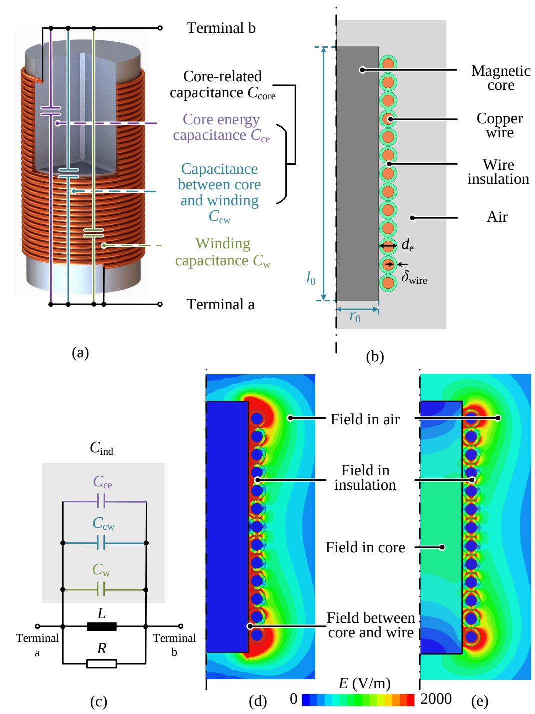

Fig. 1. Stray capacitance of high-frequency inductor. (a) Capacitance definitions. (b) Cross-section illustration. (c) Equivalent circuit. (d) Electric field of MnZn inductor (PEC model holds) (e) Electric field of NiZn inductor (PEC model not valid).

area. It can be modeled as parallel plate capacitance model with a coefficient indicating the voltage different between each turn; or modeled by calculating the stored electric field energy directly [3]. C_{cw} relates to the core and winding. It is normally modeled by the parallel plate capacitance model plus a coefficient indicating the voltage difference between each turn and the core [4–6]. The modeling of C_{ce} depends on the core permeability μ and permittivity ε which are both very high for MnZn ferrites (often, $\mu_r > 1000$ and $\varepsilon > 10,000$). If μ or ε are high, the core is regarded as a perfect electrical conductor (PEC) when calculating stored electric field energies [7]. This is illustrated in Fig. 1(d), where the electric field does not penetrate the core due to the core's high permittivity. There is little energy stored in the electric field within the core itself, therefore the core energy capacitance C_{ce} is small. By contrast, the electric field between the core and winding is strong, and C_{cw} can be large. Under the PEC assumption, the inductor's capacitance can be approximated as $C_{\mathrm{core}} = C_{\mathrm{cw}} + C_{\mathrm{ce}} \approx C_{\mathrm{cw}}$.

As frequencies increase into the HF range, NiZn ferrites are more commonly used [8–10], mainly due to their lower core loss and stable permeability [11, 12]. NiZn ferrites typically

This work was supported in part by the National Science Foundation of China under Grant 52207191, and in part by Jiangsu Provincial Key Laboratory of Smart Grid Technology and Equipment of Southeast University under Grant 4216002101. (Corresponding author: Long Jin.)

Zhan Shen, Wu Chen, and Long Jin are with the Jiangsu Provincial Key Laboratory of Smart Grid Technology and Equipment, Southeast University, Nanjing 210096, China (zhs@seu.edu.cn, chenwu@seu.edu.cn, jinlong@seu.edu.cn), Alex J. Hanson is with the Department of Electrical and Computer Engineering, The University of Texas at Austin, TX 78712 USA (ajhanson@utexas.edu), David J. Perreault is with the Department of Electrical Engineering and Computer Science, Massachusetts Institute of Technology, Cambridge, MA 02139 USA (djperrea@mit.edu), Charles R. Sullivan is with Thayer School of Engineering, Dartmouth College, NH 03755 USA (charles.r.sullivan@dartmouth.edu), Hongbo Zhao, Frede Blaabjerg, and Huai Wang are with AAU Energy, Aalborg University, Aalborg 9220, Denmark (hzh@energy.aau.dk, fbl@energy.aau.dk, hwa@energy.aau.dk).

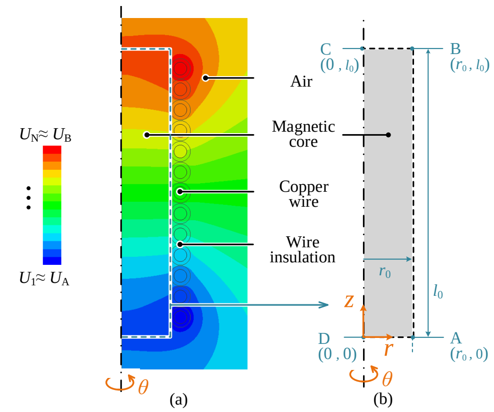

Fig. 2. Inductor structure for analytical modeling. (a) Potential distribution of a NiZn inductor with low permeability and permittivity core. (b) Core dimension, the *Unit Core Structure* is defined when $r_0 = 1$ m.

have lower permeabilities ($4 \lesssim \mu_r \lesssim 125$) and permittivities ($12 \lesssim \varepsilon \lesssim 100$) than MnZn materials [13]. Therefore, NiZn materials do not behave as perfect electrical conductors, and the PEC capacitance model does not apply. Instead, the electric field does diffuse into the core as shown in Fig. 1(e), storing non-negligible energy. We therefore make the opposite simplifying assumption from the PEC model. We assume that the electric field in the core region is comparable to the region between the winding and the core. The latter region also has a small area and smaller electricity field intensity compared with the PEC scenario. Hence, in most scenarios, the energy stored between winding and core is negligible. Mathematically, $C_{\text{core}} = C_{\text{cw}} + C_{\text{ce}} \approx C_{\text{ce}}$.

We propose two C_{ce} models for NiZn inductors with low permeability and permittivity, a general analytic model and a simplified model based on curve fitting. Both models are verified using finite element analysis (FEA) simulations and experimental results in two case studies.

II. Analytical Modeling

A. Model 1: General Analytical Field Solution

1) Problem Definition: Consider the voltage at each turn of the winding U_1, U_2, ... U_{N}, the electric field problem is then defined as Fig. 2 with three assumptions:

- The voltage between each pair of turns is the same, i.e., the voltage varies linearly across turns [14];
- For a floating core, the voltage at its surface is similar to the winding (Fig. 2(a)), therefore, the voltage along the core surface ($r = r_0$) changes linearly from U_{A} to U_{B};
- The structure and voltage are symmetrical from bottom to top, hence $U_{\text{A}} = -U_{\text{B}}$, $U_{\text{C}} = -U_{\text{D}}$ if the center of the winding is taken to be 0 volts.

The problem is then to solve Laplace's equation

$$\nabla^2 \varphi = 0 \tag{1}$$

for the electric potential distribution in the core. Using the potential, we can calculate electric field energy and capacitance.

2) Boundary Conditions: Consider solving Laplace's equation in the rectangle A-B-C-D in Fig. 2(b). The true boundary conditions for this problem offer little help toward an analytic solution. The boundary conditions are for the top and bottom edges (B-C, A-D). They only specify that each of the parallel electric field $E_{\|}$ and the normal displacement field $D_{\perp}$ must be the same on either side of the material-air boundary. The solution must therefore consider the space outside of A-B-C-D.

We propose to make the analytic problem tractable by examining the potential along the top and bottom edges (B-C, A-D) through FEA simulation, and modeling these edge potentials by curve fitting to the simulation data. We will show that, one choice of fitting function for these edge potentials yields both an accurate representation of the empirical data, and a closed-form analytic solution to Laplace's equation.

The boundary conditions will therefore be defined as:

$$\begin{aligned} \varphi|_{r=r_0} &= \left(1 - 2\frac{z}{l_0}\right) U_{\text{A}}, & \varphi|_{z=0} &= U_{\text{L}}(r), \\ \varphi|_{r=0} &= \text{finite} & \varphi|_{z=l_0} &= -U_{\text{L}}(r), \end{aligned} \tag{2}$$

where $U_{\text{L}}(r)$ is the voltage along the $z = 0$ boundary.

3) Modeling the Top and Bottom Edge Potentials $U_{\text{L}}(r)$: We simulate variations of the *Unit Core Structure* (Fig. 2(b)). They are with $r_0 = 1$ m while sweeping r_0/l_0 from 0.05 to 10 and ε from 1 to 100. In Fig. 3, note that $U_{\text{L}}(r)/U_{\text{A}}$ does not change significantly with the permittivity of the core. Therefore, we further simplify $\varepsilon = 10$ for the remainder of the analysis.

The final step in modeling $U_{\text{L}}(r)$ is to fit a curve to the simulation data, which can both provides good agreement and produces an analytically tractable boundary value problem. Observing that $U_{\text{L}}(r)$ is approximately exponential, we propose that the following function fits the data well and, as will be seen, permits an analytic solution:

$$\frac{U_{\text{L}}(r)}{U_{\text{A}}} = \begin{cases} e^{-1.513 \times (r_0 - r)/l_0 \times e^{0.574 r_0/l_0}} & \frac{r_0}{l_0} \lesssim 1 \\ e^{-2.713 \times (r_0 - r)/l_0 \times e^{0.041 r_0/l_0}} & \frac{r_0}{l_0} > 1. \end{cases} \tag{3}$$

The goodness of this function's fit can be seen in Fig. 4. The root mean square error of the fitting $\left(\text{RMSE} \triangleq \sqrt{\frac{\sum_{i=1}^{N}(data_i - model_i)^2}{N}}\right)$ is 0.0242 for $r_0/l_0 \gtrsim 1$ and 0.0418 for $r_0/l_0 \lesssim 1$. While the fit is less ideal for $r_0/l_0 \lesssim 1$, it is acceptable given the objective of generating an analytically tractable problem.

From Fig. 2 and Section II-A1, it can be concluded that for cores of different dimensions, the electric filed distributions can be scaled to the related *Unit Core Structure* of the same ε and r_0/l_0 ratio. Therefore, the ratio $U_{\text{L}}(r)/U_{\text{A}}$ obtained from (3) is applicable for rod cores of any size; $U_{\text{L}}(r)$ is obtained by multiplying (3) with U_{A}.

4) Analytical Solution: We must solve (1) with boundary conditions (2) to obtain the voltage distribution $\varphi(r, z)$. The solution to this problem is derived in Appendix A. Once the electric potential is found, the electric field strength in r and z direction are given by $E_r = -\partial\varphi(r,z)/\partial r$, $E_z = -\partial\varphi(r,z)/\partial z$. The energy of electric field ξ is then

$$\xi = \frac{1}{2}\varepsilon\varepsilon_0 \int_0^{r_0} \int_0^{l_0} 2\pi r \left(\frac{|E|}{\sqrt{2}}\right)^2 dr\, dz \tag{4}$$

and the core energy capacitance C_{ce} is

$$C_{\text{ce}} = \frac{2\xi}{(U_{\text{B}} - U_{\text{A}})^2}. \tag{5}$$

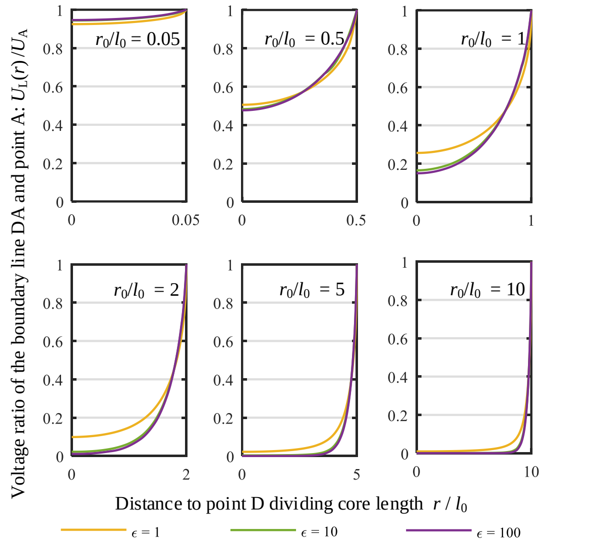

Fig. 3. $U_{\mathrm{L}}(r)/U_{\mathrm{A}}$ from simulation of the *Unit Core Structure* with different core permittivity, i.e., $\epsilon = 1$, 10, and 100.

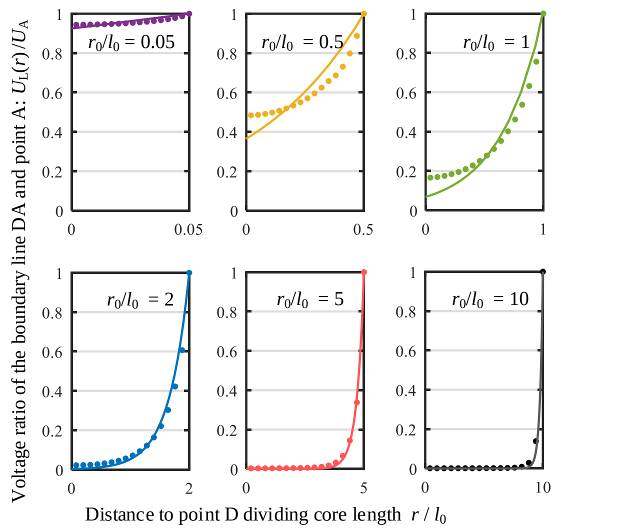

Fig. 4. Curve fitting of $U_{\mathrm{L}}(r)/U_{\mathrm{A}}$ when $\epsilon = 10$.

B. *Model 2: A Simplified Curve-Fit Model*

Model 1 and FEA simulation obtains C_{ce} by solving the electric field with the analytical method and FEA, respectively. They both require a certain computational burden. Therefore, we also propose a simplified Model 2 with only two equations and three inputs, calculating C_{ce} immediately. It is obtained by curve-fitting to simulation results of the *Unit Core Structure* with $\varepsilon = 10$, which yields the unit capacitance C_{unit}. We continue to neglect the impact of ε on the field distribution per Fig. 3. Therefore, the field distribution depends only on radius r_0 and length l_0. Calculations of C_{unit} by Model 1 and FEA simulation are shown in Fig. 5, and can be approximated as:

$$C_{\mathrm{unit}} = 156.90(1 - e^{-1.97\frac{r_0}{l_0}}) + 0.72\frac{r_0}{l_0}/(1 + e^{-8.29\frac{r_0}{l_0}}). \tag{6}$$

For a non-unit core with permittivity ε, its energy and capacitance are equal to those of the *Unit Core Structure* of the same r_0/l_0 multiplied by $\frac{\varepsilon r_0}{10}$/meter, hence the core energy capacitance C_{ce} is

$$C_{\mathrm{ce}} = \frac{\varepsilon r_0}{10} C_{\mathrm{unit}}. \tag{7}$$

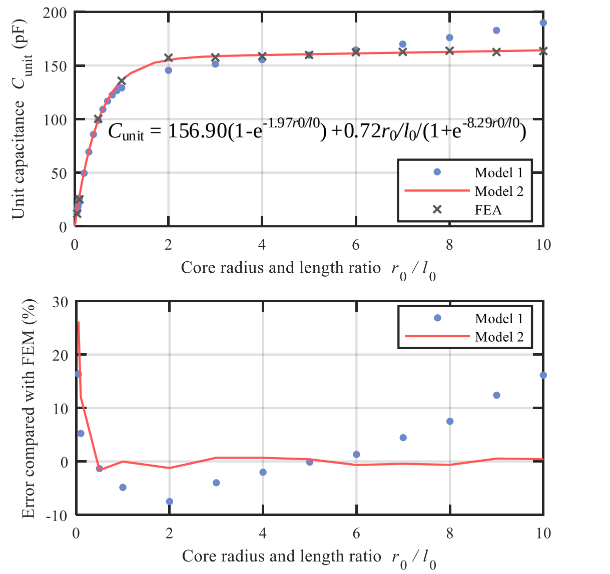

Fig. 5. Unit capacitance C_{unit} by Model 1 (General Analytical Field Solution, Section II-A), FEA and Model 2 (fit to FEA, Section II-B).

TABLE I
PARAMETERS OF INDUCTORS IN CASES 1 AND 2

	Case 1	Case 2	Units
Core length l_0	29.5	26	mm
Core radius r_0	4.9	9.9	mm
Core permeability μ	4.7	40	
Core permittivity ϵ	5.7	13	
Wire diameter d_{i}	1.7	0.812	mm
Wire insulation d_{s}	78	229	μm
Number of layers	1	1	
Number of turns	14	13	

Both models' errors from FEA are shown in Fig. 5(b). In the concerned r_0/l_0 range, the maximum error of Model 1 is below 20%, and the error comes from the imprecise modeling of the top and bottom edge potentials U_{L}(r). When $r_0/l_0 \gtrsim 2$, Model 2 has a very small error $\lesssim$2%, when $0.05 \lesssim r_0/l_0 \lesssim 2$, the maximum error is below 30%. Both models are considered acceptable.

III. Model Verification and Discussion

A. *Case 1: A Rod Core Choke*

Case 1 of a NiZn rod choke is used to verify both models, as specified in Fig. 6 and Table I with results in Fig. 7. The experimental results are obtained with Keysight impedance analyzer E4990A. The first parallel-resonant frequency f_0 and inductance value L_l are identified, and then $C_{\mathrm{ind}} = \frac{1}{L_l(2\pi f_0)^2}$ is calculated. The winding capacitance C_{w} is calculated with the model in [15]. It is the same in the PEC model and Models 1 & 2. The PEC model assumes no core energy capacitance C_{ce}, but has much higher capacitance between core and winding C_{cw}. It overestimates the overall capacitance

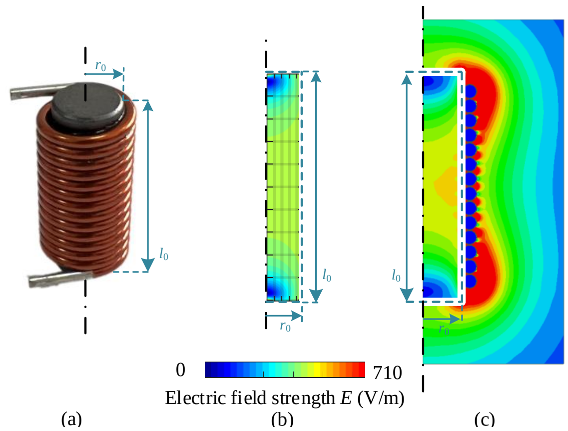

Fig. 6. Rod core choke modeling. (a) Photo of the choke. (b) Analytical electric field strength calculation plotted by Matlab. (c) Electric field strength by FEA simulation.

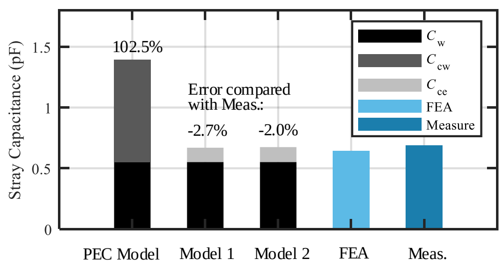

Fig. 7. Experimental verification of case 1. PEC Model refers to the Perfect Electrical Conductor model in [4] assuming a high permittivity core.

with 102.5% error. The proposed models assume $C_{\mathrm{cw}} \approx 0$, and C_{ce} is calculated by (5) and (7). The results fit well with the simulation and experiment, with only -2.7% and -2.0% error from the experiment.

B. Case 2: A Low-loss Modified Pot Core Inductor

Case 2 is a NiZn modified pot core inductor with distributed gaps for MHz application [8], specified in Fig. 8 and Table I, with results in Fig. 9. Models 1 and 2 neglect the impact of the end-caps and gaps. However, applying Models 1 and 2 to the center post and outer ring separately allows them to account for the energy in both regions. In this case study, the outer ring has a similar volume and electric field distribution as the center discs. Hence its contribution to capacitance is approximated as the same as the center core. The proposed models' errors from the experiment are 36.3% and 36.5%, which mainly due to the outer ring approximation and the quasi-distributed gap. Nevertheless, the PEC model had a much larger 205.8% error. The core energy capacitance C_{ce} makes up the majority of the inductor capacitance, emphasizing its importance.

C. Model Discussion

The analytical models in case 2 have a higher error than that in case 1. It is mainly due to the assumptions by neglecting the air gap and end caps, and approximating the outer ring core capacitance as the same as the center disc core capacitance. To improve this model, how the air gap impacts the electric field distribution in the core, how to calculate the energy in the air gap, and how to set up the boundary condition for the end caps and outer ring shall be systematically investigated in the future.

In the HF range, the electromagnetic wavelength in the core is $\lambda = \frac{1}{f\sqrt{\mu_r \mu_0 \varepsilon \varepsilon_0}}$, where f is the frequency, μ_0 and ε_0 are the permeability and permittivity of the air, respectively. Define the maximum dimension of the inductor as R, as long as $\lambda \gg R$, the electrostatic analysis can be used for capacitance modeling while the magnetic field analysis is not necessary. The impact of the permeability variation is in the magnetic field analysis and therefore can be neglected. In this paper, in *case 1*, (λ = 1931 mm at 30MHz) $\gg$ (R= 29.5 mm); in *case 2*, (λ = 970 mm at 13.56 MHz) $\gg$ (R= 26 mm) , hence the assumption of using electrostatic analysis is reasonable. Finally, the proposed two models are for NiZn cores with low μ and ε; for MnZn core with much higher μ and ε [16, 17], the time-varying electromagnetic analysis of the electric field is necessary to calculate C_{ce}.

The core permittivity ε can change with the frequency, and based on our field distribution analysis in Fig. 2, Fig. 3, and Section II-A1, the field distribution of the core does not vary significantly with ε when $1 \lesssim \varepsilon \lesssim 100$. Hence the proposed two models works well in this range and the accuracy decreases when ε increases beyond 100.

Model 1 is a general solution for any core structures with different boundary conditions, and Model 2 is only for the rod core structure. Although the boundary condition and Model 2 in this paper are obtained by curve fitting of *Unit Rod Core Structure*, the presented two modeling methods are general and can be extended to other core structures. For instance, for the planar/EE type core, its cross-section is similar as the cross-section of the modified pot core in Fig. 8, therefore similar assumptions and modeling methods can be applied. For the toroidal cores, the voltage boundary conditions of their toroidal cross-sections can be assumed same as the attached winding. Hence, together with Laplace's equation, the core energy capacitance can be obtained with Model 1. Moreover, their electric field distributions are the same for different core dimensions if their toroidal cross-sections have the same outer/inner radius ratio. Therefore, the core energy and capacitance of those cores are proportional to each other with the ratio of ε and their radius. The curve fitting method as Model 2 can also be used by defining the *Unit Toroidal Core Structure*.

IV. Conclusion

We proposed an analytic model and a curve-fit model for NiZn inductors with low core permeability and permittivity, where the electric field in the core cannot be neglected. Simulation and experimental results verify both models in two case studies with significant error reduction compared with the conventional model.

Appendix A
Derivation of the Electric field potential

Let the original voltage distribution subtracts $\varphi'' = (1 - 2\frac{z}{l_0})U_{\mathrm{A}}$, the boundary condition and problem transfer to

$$\varphi'|_{r=r_0} = 0, \qquad \varphi'|_{z=0} = U'_{\mathrm{L}}(r), \tag{A.1}$$

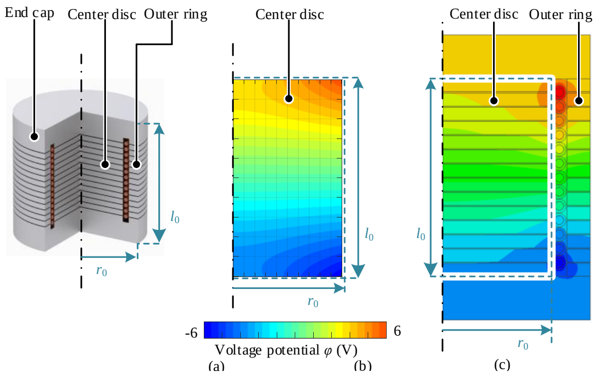

Fig. 8. Modified pot core inductor modeling. (a) Photo of the inductor. (b) Analytical voltage distribution calculation plotted by Matlab. (c) Voltage distribution plotted by FEA simulation.

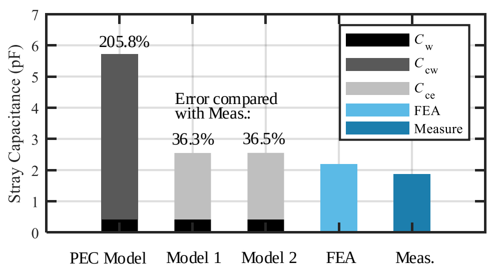

Fig. 9. Experimental verification of case 2.

$$\varphi'|_{r=0} = \text{finite}\varphi'|_{z=l_0} = -U'_{\mathrm{L}}(r), \tag{A.2}$$

$$\nabla^2\varphi' = 0 \tag{A.3}$$

where $U'_{\mathrm{L}}(r) = U_{\mathrm{L}}(r) - \varphi''$.

The general solution to the problem is [18]

$$\varphi' = A_0 + B_0 z + \sum_{n=1}^{\infty}(A_{\mathrm{n}}e^{x_{\mathrm{n}}^{(0)}z/r_0} + B_{\mathrm{n}}e^{-x_{\mathrm{n}}^{(0)}z/r_0})J_0(\frac{x_{\mathrm{n}}^{(0)}}{r_0}r). \tag{A.4}$$

Combing the boundary conditions (A.1, A.2) obtains

$$\begin{cases} A_0 = 0, \qquad A_{\mathrm{n}} = \frac{G_{1\mathrm{n}}e^{-x_{\mathrm{n}}^{(0)}l_0/r_0} - G_{2\mathrm{n}}}{e^{-x_{\mathrm{n}}^{(0)}l_0/r_0} - e^{x_{\mathrm{n}}^{(0)}l_0/r_0}} \\ B_0 = 0, \qquad B_{\mathrm{n}} = \frac{G_{1\mathrm{n}}e^{x_{\mathrm{n}}^{(0)}l_0/r_0} - G_{2\mathrm{n}}}{e^{x_{\mathrm{n}}^{(0)}l_0/r_0} - e^{-x_{\mathrm{n}}^{(0)}l_0/r_0}} \\ G_{1\mathrm{n}} = \frac{2}{r_0^2[J_0(x_{\mathrm{n}}^{(0)})]^2}\int_0^{r_0} U'_{\mathrm{L}}J_0(\frac{x_{\mathrm{n}}^{(0)}}{r_0}r)r\,dr \\ G_{2\mathrm{n}} = \frac{2}{r_0^2[J_0(x_{\mathrm{n}}^{(0)})]^2}\int_0^{r_0} -U'_{\mathrm{L}}J_0(\frac{x_{\mathrm{n}}^{(0)}}{r_0}r)r\,dr \end{cases} \tag{A.5}$$

where J_0 and J_1 are the Bessel function of first kind in order of 0 and 2, $x_{\mathrm{n}}^{(0)}$ is the n-th positive zero of J_1, respectively.

The final solution of $\varphi(r, z)$ is

$$\varphi(r, z) = \varphi'(r, z) + \varphi'' = \varphi'(r, z) - \frac{2U_{\mathrm{A}}}{l_0}z + U_{\mathrm{A}}. \tag{A.6}$$

References

[1] D. J. Perreault, J. Hu, J. M. Rivas, Y. Han, O. Leitermann, R. C. N. Pilawa-Podgurski, A. Sagneri, and C. R. Sullivan, "Opportunities and challenges in very high frequency power conversion," in *Proc. IEEE APEC*, 2009, pp. 1–14.

[2] M. A. Saket, N. Shafiei, and M. Ordonez, "LLC converters with planar transformers: Issues and mitigation," *IEEE Trans. Power Electron.*, vol. 32, no. 6, pp. 4524–4542, Jun. 2017.

[3] J. Biela and J. W. Kolar, "Using transformer parasitics for resonant converters-a review of the calculation of the stray capacitance of transformers," *IEEE Trans. Ind. Appl.*, vol. 44, no. 1, pp. 223–233, Jan. 2008.

[4] Z. Shen, H. Wang, Y. Shen, Z. Qin, and F. Blaabjerg, "An improved stray capacitance model for inductors," *IEEE Trans. Power Electron.*, vol. 34, no. 11, pp. 11 153–11 170, Nov. 2019.

[5] H. Zhao, D. N. Dalal, A. B. Jorgensen, J. K. Jorgensen, X. Wang, S. Beczkowski, S. Munk-Nielsen, and C. Uhrenfeldt, "Physics-based modeling of parasitic capacitance in medium-voltage filter inductors," *IEEE Trans. Power Electron.*, vol. 36, no. 1, pp. 829–843, Jan. 2020.

[6] B. Liu, R. Ren, F. Wang, D. Costinett, and Z. Zhang, "Winding scheme with fractional layer for differential-mode toroidal inductor," *IEEE Trans. Ind. Electron.*, vol. 67, no. 2, pp. 1592–1604, Feb. 2020.

[7] W. Tan, "Modeling and design of passive planar components for EMI filters," Ph.D. dissertation, Lille, France: Ecole Centrale de Lille, 2012.

[8] R. S. Yang, A. J. Hanson, B. A. Reese, C. R. Sullivan, and D. J. Perreault, "A low-loss inductor structure and design guidelines for high-frequency applications," *IEEE Trans. Power Electron.*, vol. 34, no. 10, pp. 9993–10 005, Oct. 2019.

[9] R. S. Bayliss, R. S. Yang, A. J. Hanson, C. R. Sullivan, and D. J. Perreault, "Design, implementation, and evaluation of high-efficiency high-power radio-frequency inductors," in *Proc. IEEE APEC*, 2021, pp. 881–888.

[10] P. Thummala, D. B. Yelaverthi, R. A. Zane, Z. Ouyang, and M. A. E. Andersen, "A 10-mhz ganfet-based-isolated high step-down dc-dc converter: Design and magnetics investigation," *IEEE Trans. Ind. Appl.*, vol. 55, no. 4, pp. 3889 –3900, Jul. 2019.

[11] F. C. Lee and Q. Li, "High-frequency integrated point-of-load converters: Overview," *IEEE Trans. Power Electron.*, vol. 28, no. 9, pp. 4127–4136, Sep. 2013.

[12] A. J. Hanson, J. A. Belk, S. Lim, C. R. Sullivan, and D. J. Perreault, "Measurements and performance factor comparisons of magnetic materials at high frequency," *IEEE Trans. Power Electron.*, vol. 31, no. 11, pp. 7909–7925, Nov. 2016.

[13] Ferroxcube, "Soft ferrites - ferrite materials survey," Tech. Rep., 2008, Available: https://ferroxcube.home.pl/prod/assets/sfmatgra_frnt.pdf.

[14] H. Zhao, S. Luan, Z. Shen, A. J. Hanson, Y. Gao, D. N. Dalal, R. Wang, S. Zhou, and S. Munk-Nielsen, "Rethinking basic assumptions for modeling parasitic capacitance in inductors," *IEEE Trans. Power Electron.*, vol. 37, no. 7, pp. 8281–8289, 2022.

[15] G. Grandi, M. K. Kazimierczuk, A. Massarini, and U. Reggiani, "Stray capacitances of single-layer solenoid air-core inductors," *IEEE Trans. Ind. Appl.*, vol. 35, no. 5, pp. 1162–1168, Sep. 1999.

[16] C. Cuellar, W. Tan, X. Margueron, A. Benabou, and N. Idir, "Measurement method of the complex magnetic permeability of ferrites in high frequency," in *Proc. IEEE I2MTC*, 2012, pp. 63–68.

[17] Y. Li and S. Wang, "Modeling and increasing the high-frequency impedance of single-layer Mn-Zn ferrite toroidal inductors with electromagnetic analysis," *IEEE Trans. Power Electron.*, vol. 36, no. 6, pp. 6943–6953, 2021.

[18] M. Zahn, *Electromagnetic field theory: a problem solving approach*. Cambridge, MA, USA: Massachusetts Institute of Technology, 1979.